

Morphology and magnetism of multifunctional nanostructured γ -Fe₂O₃ films: Simulation and experiments

R.F. Neumann* and M. Bahiana

*Instituto de Física, Universidade Federal do Rio de Janeiro,
Caixa Postal 68528, Rio de Janeiro 21941-972, Brazil*

L.G. Paterno and M.A.G. Soler

Universidade de Brasília, Instituto de Física, Brasília DF 70910-900, Brazil

J.P. Sinnecker

Centro Brasileiro de Pesquisas Físicas, Rio de Janeiro RJ 22290-180, Brazil

J.G. Wen

University of Illinois at Urbana-Champaign, Frederick Seitz Materials Research Laboratory, Urbana IL 61808, USA

P.C. Morais

Universidade de Brasília, Instituto de Física, Brasília DF 70910-900, Brazil

(Dated: September 1, 2011)

This paper introduces a new approach for simulating magnetic properties of nanocomposites comprising magnetic particles embedded in a non-magnetic matrix, taking into account the 3D structure of the system in which particles' positions correctly mimic real samples. The proposed approach develops a multistage simulation procedure in which the size and distribution of particles within the hosting matrix is firstly attained by means of the Cell Dynamic System (CDS) model. The 3D structure provided by the CDS step is further employed in a Monte Carlo (MC) simulation of zero-field-cooled/field-cooled (ZFC/FC) and magnetic hysteresis loops ($M \times H$ curves) for the system. Simulations are aimed to draw a realistic picture of the as-produced ultra-thin films comprising maghemite nanoparticles dispersed in polyaniline. Comparison (ZFC/FC and $M \times H$ curves) between experiments and simulations regarding the maximum of the ZFC curve (T_{MAX}), remanence (M_R/M_s) and coercivity (H_C) revealed the great accuracy of the multistage approach proposed here while providing information about the system's morphology and magnetic properties. For a typical sample the value we found experimentally for T_{MAX} (54 K) was very close to the value provided by the simulation (53 K). For the parameters depending on the nanoparticle clustering the experimental values were consistently lower ($M_R/M_s = 0.32$ and $H_C = 210$ Oe) than the values we found in the simulation ($M_R/M_s = 0.53$ and $H_C = 274$ Oe). Indeed, the approach introduced here is very promising for the design of real magnetic nanocomposite samples with optimized features.

PACS numbers: 75.70.-i, 75.75.-c, 75.75.Cd, 75.47.Lx, 02.70.Uu, 05.10.Ln

I. INTRODUCTION

Assemblies of nanoscaled particles or clustered nanosized systems have attracted a great deal of interest either due to their fundamental properties or their potential use in several technological applications^{1,2}. In particular, composites containing nanosized magnetic particles dispersed in a hosting matrix can be envisaged as multifunctional materials with promising applications in emerging fields³⁻⁵. In this particular class of material system isolated magnetic particles are sufficiently small, so that they usually remain in a single-domain magnetic state⁶. Nonetheless, it is possible to modulate the particle-particle interaction over a broad range of magnetic particle concentration in such a way that inter-particle interaction starts playing a significant role on the nanocomposite end properties^{7,8}. Different types of magnetic interactions are found in nanoparticulated systems, including the magnetic dipole coupling; the indirect exchange or Rudermann-Kittel-Kasuya-Yosida (RKKY) interaction mediated by conduction electrons, for instance when the matrix and particles are both metallic; the short-range direct exchange interaction when surfaces of neighbor nanoparticles are in close contact; and the tunneling exchange interaction, which occurs when nanoparticles are considered to be only some tenths of nanometers apart from one another^{9,10}.

Besides the complexity of the dipolar interaction there is also an uncertainty in determining the anisotropy axis direction and location of the magnetic nanoparticle within the nanocomposite matrix. However, advances in theoretical, experimental and simulation have contributed to unveil the magnetic behavior of one and two dimensional systems of interacting particles¹¹⁻¹⁹. Monte Carlo (MC) simulations have been used to assess the magnetic properties of nanocomposites comprising iron oxide-based nanosized particles embedded in non-magnetic matrices. Buján-Núñez

et al.²⁰ studied the influence of the nanoparticle size on the blocking temperature of interacting systems (dipole-dipole interaction) using MC simulation of zero-field-cooled curves. Hoppe et al.²¹ employed a similar method to study the influence of the dipolar interaction on the blocking temperature of a random array of superparamagnetic particles (maghemite) dispersed within different polymeric matrices. Lamba and Annapporni²² reported simulation results including effects of disorder, short-range exchange, long-range dipolar interaction and anisotropy effects, using parameters of a maghemite-based system.

It becomes clear that the simulation of the magnetic response of realistic 3D systems of interacting nanoparticles is mandatory to understand the relationship between the nanocomposite structure and its magnetic properties. Despite efforts expended to address this issue not many investigations have been developed with great level of detail. For instance, assemblies of monodisperse particles placed at lattice positions have been used to describe experimental systems with much more complex morphology. Another possible approach, but rather inefficient, sorts particle sizes from a distribution and places them at random positions. Since particles cannot overlap, the rejection frequency for new positions gets higher while the sample becomes denser and, consequently, the algorithm becomes very slowly.

In the present study we propose an alternative approach, a multistage simulation in which the 3D spatial structure of a nanocomposite system comprising magnetic nanoparticles dispersed within a non-magnetic matrix is firstly generated by means of the Cell Dynamic System (CDS) model^{23,24}. With the use of an iterative algorithm the model is capable of generating the main systems features, namely particle positions, sizes, and shapes. In a second step, the generated 3D structure is employed in the MC simulation of zero-field-cooled/field-cooled (ZFC/FC) curves and hysteresis loops. The simulated 3D structure and the corresponding magnetic properties are then compared with the experimental data recorded from real samples, namely ultra-thin films of polyaniline (PANI) encapsulating citrate-coated maghemite (cit-MAG) nanoparticles. Our findings successfully proved that the computational approach employed in the present study can be used to assess, with great accuracy, even for more complex systems, the major morphological and magnetic features of the real samples. A similar approach has been used in simulation of ZFC-FC curves of CuCo films¹³, but in this case the simulated sample was two-dimensional and the cobalt nanoparticles had a broad size dispersion and no local order.

II. EXPERIMENTAL PROCEDURE

A. Synthesis of Nanoparticle dispersions and Preparation of Nanostructured Films

Magnetic nanocomposites were produced via the layer-by-layer (LbL) technique following the procedure previously reported^{25,26}, in which layers of anionic citrate-coated maghemite (cit-MAG) nanoparticle and cationic polyaniline (PANI) were alternately and electrostatically adsorbed onto a solid substrate. The cit-MAG suspension was prepared in a two-step chemical route as reported elsewhere²⁷ and briefly described as follows. In the first step Fe(II) and Fe(III) ions were co-precipitated in alkaline medium to produce magnetite nanoparticle, which was oxidized to produce maghemite. In the second step, the as-produced maghemite nanoparticles were rendered negatively charged via functionalization with excess of citric acid and suspended as an aqueous-based magnetic fluid sample. The doped PANI solution was prepared by dissolution of a commercial undoped PANI (Mw 10,000 g mol⁻¹, Aldrich, USA) in a mixture of N',N"-dimethylacetamide and hydrochloridric aqueous solution (pH 2.7). The nanocomposite production was realized by alternate and successive immersions of hydrophilic (100)-oriented Si stripes into PANI (polycation) and cit-MAG (anion) solutions. In between immersions substrates were rinsed in a stirred bath of HCl solution (pH 2.7) and dried with N₂ flow. Multilayered magnetic nanocomposite films of (PANI/cit-MAG)_ℓ, with ℓ increasing from 1 to 50 bilayers, were produced by repeating the cycles described above. Samples with ℓ = 10, 25 and 50 were systematically investigated. All LbL depositions were carried out at room temperature (≈ 25 °C).

B. Measurements and Instruments

Surface morphology of the thin composite films was characterized with scanning electron microscope (SEM) (Hitachi S4800). Transmission electron microscopy (TEM) micrographs were recorded with a 200 kV instrument (JEOL JEM 2100) to evaluate the average particle size and size distribution of nanoparticles in the magnetic fluid sample as well as their distribution within the nanocomposite films (cross-section images). Figure 1(a) shows the surface morphology of a (PANI/cit-MAG)₁₀ film, with nano cit-MAG spheres with little size dispersion and local HCP packing.

Values of the average particle diameter ($D_{\text{TEM}} = 7.5 \pm 0.1$ nm) and standard diameter deviation ($\sigma = 0.33 \pm 0.03$ nm) of the suspended magnetic particles (magnetic fluid sample) were obtained after fitting the particle size histogram using a log-normal distribution function, as described in the literature²⁸. Preparation of the Si substrate-deposited

nanocomposite films for cross-sectional TEM observation followed the standard protocol: films were firstly glue face-to-face, then Si substrate was mechanically ground down to about 20 μm in thickness, following the ion milling of the sample to perforation. The resulting histogram can be seen in Fig. 2(a).

Magnetic properties of the nanocomposite samples, at different applied fields and temperatures, were measured using a Cryogenics S600 SQUID magnetometer. The diamagnetic correction was taken into account while analyzing the data. For the ZFC/FC measurements the samples, as well as the measuring system magnet, were initially demagnetized at room temperature, ensuring the zero field condition. After demagnetization samples were cooled down to 2 K when the measuring field (36 Oe) was turned on. The ZFC measurements were taken while heating the sample at a constant rate of 1 K/s. After reaching room temperature, the sample was cooled down to 2 K again, without switching off the measuring magnetic field (36 Oe). FC measurements were taken while heating the sample at the same rate (1 K/s). Magnetization (M) versus field (H) hysteresis loops were taken at different fixed temperatures (2 and 300 K). The total magnetization of each nanocomposite sample was scaled to the %wt content of cit-MAG, the latter obtained from UV-vis spectroscopy (Shimadzu spectrophotometer, model UVPC 1600). The %wt contents of cit-MAG within the nanocomposite samples were obtained by measuring their optical absorption at 480 nm wavelength. The cit-MAG contents were determined from a previously constructed calibration curve based on the absorbance values of cit-MAG suspensions, at different nanoparticle concentrations and at 480 nm, which corresponds to the typical wavelength for electronic transitions in iron oxides²⁹.

III. SIMULATION

The simulation procedure comprises three main stages: generation of the spatial structure, attribution of the magnetic properties and simulation of magnetization curves. For each part different computational techniques were used, as described below.

A. Three dimensional simulation of the samples morphology

The (PANI/cit-MAG) $_{\ell}$ nanofilms investigated are a typical binary system with nanosized magnetic particles embedded in a polymeric matrix. The PANI phase surrounding cit-MAG nanoparticles prevents particle clustering leading to a structure with some regularity in terms of particle shape and position. In this binary material system, the sample can be idealized as an array of isolated spheres, with a well-defined size distribution, packed in a local HCP order and presenting long-range disorder. The pattern observed in the film cross-sectional micrograph resembles those in samples consisting of microphase separated diblock copolymers, in which one of the polymer subchains is much longer than the other one. This similarity motivated us to select the CDS model for the phase segregation of block copolymers to simulate the morphology of the as-produced nanostructured magnetic films. The CDS technique was originally proposed by Oono and Puri^{23,24} and has been successfully employed to simulate the spatial structure of block copolymers³⁰ with great computational efficiency. Let us remind that the polymeric matrix itself surrounding the maghemite nanoparticles we study in this paper has no relation with the diblock copolymers that served as an inspiration for the use of the CDS technique. It is only the final pattern generated by the CDS numerical algorithm that resembles the (PANI/cit-MAG) $_{\ell}$ nanofilms, thus motivating us to use this specific technique.

The CDS technique proposes models discrete in time and space. It is based on the sequential iteration of diffusely coupled maps that mimic the local segregation dynamics in terms of a local order parameter, $\psi(\vec{r}, t)$, providing the number density difference between the two segregating species at the position \vec{r} and time t . Non-segregated regions correspond to cells in which $\psi \approx 0$. Segregated domains have either $\psi > 0$ or $\psi < 0$, depending upon the predominant species. In the present case we have nanoparticles with fixed sizes, so we must seek a model in which the final segregated pattern has the same characteristic. Although the model provides the time evolution of the segregation process, we are interested only in the final pattern consisting of roughly spherical particles placed in a matrix with some local order. The iteration procedure converges to this pattern very quickly, so the method is extremely efficient.

In the present study we consider a three dimensional lattice with periodic boundary conditions along all directions. The order parameter was defined such that the final pattern had spherical domains with $\psi < 0$ (maghemite nanoparticles) in a background with $\psi > 0$ (polymeric matrix). The system was initialized with $\psi(\vec{r}, t) = \psi_0 + \alpha(\vec{r})$, where ψ_0 is the off-criticality and α is a random number in the interval $[-0.005, 0.005]$. The order parameter at time $t + 1$ is computed from the previous one according to Eq. 1:

$$\psi(\vec{r}, t + 1) = \psi(\vec{r}, t) - \nabla^2 [I(\vec{r}, t)] + B [\psi_0 - \psi(\vec{r}, t)], \quad (1)$$

where

$$I(\vec{r}, t) = A \tanh [\psi(\vec{r}, t)] - \psi(\vec{r}, t) + \Gamma \nabla^2 [\psi(\vec{r}, t)]. \quad (2)$$

Here, $A > 1$ is the segregation strength and defines the maximum absolute value of ψ . Γ is a phenomenological diffusion constant and the parameter $B \ll 1$ is responsible for the partial segregation. The symbol ∇^2 stands for the three-dimensional isotropic discrete Laplacian defined as³¹:

$$\nabla^2[f(\vec{r})] = \left[\frac{6}{80} \sum_{nn} f(\vec{r}_{nn}) + \frac{3}{80} \sum_{nnn} f(\vec{r}_{nnn}) + \frac{1}{80} \sum_{nnnn} f(\vec{r}_{nnnn}) \right] - f(\vec{r}), \quad (3)$$

where the subscripts nn, nnn and nnnn stand for “nearest-neighbor”, “next-nearest-neighbor” and “next-next-nearest-neighbor”, respectively.

The spatial structure to be analyzed was simulated by iterating 2000 times Eqs. 1 and 2 on a $300 \times 300 \times 30$ slab, with the 300×300 planes parallel to the xy plane. In all simulations we used the parameter values that are known to generate the pattern we are looking for³⁰: $\psi_0 = 0.3$, $A = 1.3$, $\Gamma = 0.5$, and $B = 0.02$.

B. Analysis of the simulated morphology

After the CDS simulation one has the values of order parameter for all cells. The next step is to convert this information into N_p sets of parameters $\{\vec{r}_i, \vec{m}_i, K_i^S, \hat{e}_i\}$ defined as position (\vec{r}_i), total magnetic moment (\vec{m}_i), shape anisotropy constant (K_i^S) and easy magnetization axis (\hat{e}_i) for each nanoparticle.

The first step is to identify the particles. For that, a three-dimensional extension of the Hoshen & Kopelman algorithm³² for cluster identification and labeling was used. This analysis led to the total number of clusters (N_p) and to the number of cells belonging to each cluster ($\{n_i\}$). Afterwards, we determined the clusters positions by calculating the center of mass of the group of cells forming each cluster. Next comes the analysis of the particles shape for determination of shape anisotropy properties (easy axis direction and strength) of each cluster. We considered that the particles had a prolate ellipsoidal shape. In this case the shape anisotropy constant could be calculated as follows³³:

$$K^s = \left(\pi - \frac{3}{4} N_c \right) M_s^2, \quad (4)$$

with

$$N_c(r = c/a) = \frac{4\pi}{(r^2 - 1)} \left[\frac{r}{\sqrt{r^2 - 1}} \ln \left(r + \sqrt{r^2 - 1} \right) - 1 \right], \quad (5)$$

where a and c are lengths of the shorter and longer particle axis, respectively. The ratio $r = c/a$ and the easy axis direction can be determined by diagonalizing the inertia matrix for each particle.

Another issue is the calibration of the length scale. The pattern generated by the CDS model has an arbitrary length scale. In order to obtain a good quantitative comparison with experiment we calibrated the simulated pattern by defining that the simulated average diameter (D_{CDS}) had the same value as in the real sample (D_{TEM}), that is $D_{\text{CDS}} \cong 7.5$ nm. With this, the length of each cell is

$$l_{\text{cell}} = D_{\text{TEM}} \left(\frac{\pi}{6\bar{n}_c} \right)^{\frac{1}{3}}, \quad (6)$$

where \bar{n}_c is the average number of cells in the clusters. The magnetic moment of each cluster depends on its number of cells (n_i) and can be obtained from the experimental value of the saturation magnetization (M_s) through $|\vec{m}_i| = M_s n_i l_{\text{cell}}^3$. For this simulated system, the average shape anisotropy constant was $\langle K^s \rangle = 7.2 \times 10^4$ erg/cm³ as calculated through Eq. 4. The simulated particle size distribution in the ensemble is presented in Fig. 2(b).

C. Monte Carlo simulation

In order to proceed with the simulation of the magnetization curves it is necessary to specify which energy terms will be taken into account in the MC simulation. According to our simulated ensemble, the distance R_{nn} between grains was relatively large, so that inter-particle interaction, such as direct exchange and RKKY, were neglected. Within this approximation, the magnetic dipolar interaction was the only considered one among particles. We wrote down this interaction in terms of magnetic dipoles positioned at the center of the particles. Finally, the anisotropy energy

included shape and crystalline contributions. Including the terms mentioned above we defined the total energy of the N_p particles in the presence of an external magnetic field (\vec{H}) as:

$$E = \sum_{i=1}^{N_p} \left[-\vec{m}_i \cdot \vec{H} + E_i^A + \sum_{j>i}^{N_p} \frac{\vec{m}_i \cdot \vec{m}_j - 3(\vec{m}_i \cdot \hat{r}_{ij})(\vec{m}_j \cdot \hat{r}_{ij})}{|\vec{r}_{ij}|^3} \right], \quad (7)$$

where the first term denotes the particles Zeeman term and E_i^A accounts for shape and crystalline anisotropy energies. Based on the experimental data available from the literature^{34–41} we have assumed uniaxial crystalline anisotropy for cubic maghemite, thus using the value $K_u = 1.25 \times 10^5$ erg/cm³ in the simulations. Note that the third term in Eq. 7 refers to the particle-particle dipolar interaction, in which \vec{r}_{ij} defines the distance between particles i and j . In order to mimic the nanocomposite film we have applied periodic boundary conditions for the magnetostatic interaction on the xy plane.

The MC simulations were performed using the Metropolis algorithm. In short, a new orientation for the magnetic moment of a randomly chosen nanoparticle is set, then the energy difference (ΔE) between old and new orientations is calculated and accepted with probability $p = \min[1, \exp(-\Delta E/k_B T)]$. The new orientation for the magnetic moments is chosen according to an algorithm analogous to the one proposed by Nowak et al.⁴², in which a randomly oriented vector \vec{v} with modulus $G|\vec{m}_i|$ is added to the moment \vec{m}_i . By changing G one can control how different new and old directions might be. With this algorithm the magnetic moment is restricted to a cone centered in \vec{m}_i with an opening angle $\theta_{\max} = \sin^{-1}(G)$ (see Fig. 3). We have used $\theta_{\max} = 15^\circ$ throughout the simulation. One MC step (MCS) corresponds to examining, in average, all the magnetic moments.

IV. RESULTS AND DISCUSSION

Figure 1 shows the experimental (a) and simulated spatial structures (b). A qualitative analysis shows good agreement between both structures. Following with the morphology comparison, we calculated the size histogram that was well fitted by a log-normal distribution with $\sigma = 0.11$ nm. Simulated and experimental histograms are shown in Fig. 2 and the comparison between them reinforces the adequacy of the simulated sample. Finally we calculated the pair correlation function, $g(r)$, from which one can estimate the average distance between nearest-neighbors (R_{nn}). Figure 4(b) displays $g(r)$ and clearly indicates short-range order at distances smaller than 30 nm. From the first $g(r)$ peak position we concluded that the average center-to-center nearest neighbor distance is $R_{nn} = 10$ nm. Considering that the average particle diameter is 7.5 nm, the average interparticle separation is about 2.5 nm. In the real sample this number represents the average distance of neighboring particles, that is a surface-to-surface spacing of about 2.5 nm, which is filled by the hosting polymeric material, in very good agreement with the observed TEM cross-sectional micrographs in Fig. 4(a).

The simulated ZFC/FC curves were obtained starting from a demagnetized state at 2 K. The temperature was then increased at a rate of $\nu = 50$ MCS/2K, up to 300 K, under an applied in-plane magnetic field of 36 Oe. Here MCS stands for Monte Carlo steps. For the simulation of the FC curve we started the simulation with the last configuration of the ZFC curve and the temperature was decreased down to 2 K at the same rate as in the ZFC curve. This procedure was repeated 2000 times and the results were averaged out over all statistically equivalent realizations. For simplification we have considered $K_i^S = \langle K^S \rangle$ (its average over the ensemble). Experimental and simulated ZFC/FC curves are presented in Figures 5(a) and 5(b), respectively. The values of T_{MAX} in the ZFC curves were 54 and 53 K for the experimental and simulated curves, respectively. Since T_{MAX} scales with the blocking temperature T_B we can draw conclusions about the amount of interaction in the samples through the variation of T_{MAX} . The decreasing of ℓ (the number of bilayers) in the (PANI/cit-MAG) $_{\ell}$ magnetic nanocomposite films, causes the reduction of T_{MAX} from 54 K ($\ell = 50, 25$) to 45 K ($\ell = 10$). This is consistent with the picture of particle interaction effects reported in the literature⁴³ as the content of the magnetic nanoparticle incorporated within (PANI/cit-MAG) $_{\ell}$ reduces with the reduction of ℓ . The small discrepancy in T_{MAX} from 53 K (simulated) in comparison to 54 K (experimental), as shown in Figures 5, indicates that the two samples (simulated and experimental) are indeed quite similar, though the real sample might present stronger particle-particle interaction than the simulated one. Interesting to note that $T_{\text{MAX}} = 54$ K was observed in both nanocomposite films ($\ell = 50, 25$), indicating that the nanoparticle packing has reached a limit and the only difference between the two samples is actually the film thickness. Furthermore, while comparing with the simulated ZFC/FC curves the observed flattening of the experimental ZFC/FC curves ($\ell = 10, 25, 50$) indicates the mean-field effect, more likely due to the increasing of the samples demagnetizing factor as a consequence of the particle chain formation⁴³. While the simulated ZFC/FC curves shown in Fig. 5(b) were derived from a system comprising an ensemble of single nanoparticles, though including dipolar interaction among them, as described in Eq. 7, the experimental data do indicate that particle clustering takes place in the real samples we investigated here.

The discussion regarding the data provided by the ZFC/FC curves is corroborated by the experimental ($\ell = 25$) and simulated hysteresis curves shown in Figures 6(a) and 6(b), respectively. Simulations of hysteresis cycles were performed at $T = 2$ and 300 K while applying an in-plane magnetic field. For the simulated cycles the saturation field H_s was determined as the field at which the magnetization reaches 99% of the sample's saturation magnetization. After reaching saturation the in-plane applied field was swept between $+H_s$ and $-H_s$ at a rate of $\nu = 100$ MCS/10 Oe. Notice the similarity of the room temperature ($T = 300$ K) reduced remanence values for the experimental ($M_r/M_s = 0.54$) and simulated ($M_r/M_s = 0.49$) curves, shown in Figure 6. Additionally, notice the similarity of the experimental and simulated hysteresis cycles at $T = 300$ K, with minimal remanence (M_R) and coercivity (H_C). Nevertheless, the low temperature ($T = 2$ K) reduced magnetization, remanence and coercivity values observed in the data provided by Figures 6(a) and 6(b) are quite different. We found the experimental and simulated normalized magnetization (M^*/M_s) at $H^* = 1$ kOe equal to 0.61 and 0.93, respectively. This is a clear indication that particle clustering takes place in the real (PANI/cit-MAG)₂₅ sample. In support to this model picture we found the experimental normalized magnetization (M^*/M_s) at $H^* = 1$ kOe equals to 0.68 for the (PANI/cit-MAG)₁₀ sample, indicating reduced particle clustering as the particle concentration reduces (from $\ell = 25$ down to $\ell = 10$) within the magnetic nanocomposite film. Additionally, from Figure 6 we found the experimental and simulated low temperature ($T = 2$ K) reduced remanence (M_R/M_s) equal to 0.32 and 0.53, respectively. The simulated value of $M_R/M_s = 0.53$ is very much closer to the value predicted by the Stoner-Wohlfarth theory ($M_R/M_s = 0.50$) of non-interacting uniaxial single domain particles at $T = 0$ K⁴⁴.

On the other hand, particle-particle interaction is expected to reduce the values of M_R/M_s ⁴⁵, as observed in the nanocomposite films investigated here. In agreement with the discussion above we found for the (PANI/cit-MAG)₁₀ sample $M_R/M_s = 0.35$ at $T = 2$ K, confirming the reduced particle content within the magnetic nanocomposite film of this sample in comparison with the (PANI/cit-MAG)₂₅ sample. Likewise, the analysis of the coercivity (H_C) values obtained from the data shown in Figure 6 reveals the expected tendency of enhancement with reduction of the particle-particle interaction⁴⁵. The low temperature ($T = 2$ K) values of coercivity observed in the experimental and simulated curves shown in Figures 6(a) and 6(b) were $H_C = 210$ and $H_C = 274$ Oe, respectively.

A final comment regarding the success of the simulation approach developed herein is based on the correlation function presented in Fig. 4. From Fig. 4b we found the system is order up to about 30 nm in length, indicating that we should expect a tendency of saturation of the magnetic properties which are dependent upon the particle-particle interaction in nanocomposite films (like ours) with thicknesses higher than about 30 nm. Recently, we found the thickness of the (PANI/cit-MAG) _{ℓ} system linearly increasing with ℓ , the slope increasing with the concentration of the suspended nanoparticles within the magnetic fluid sample used for fabricating the films²⁶. Indeed, we observed T_{MAX} , M_R/M_s and H_C systematically changing as one goes from sample (PANI/cit-MAG)₁₀ to sample (PANI/cit-MAG)₂₅. Nevertheless, only slight changes in all these values (T_{MAX} , M_R/M_s and H_C) were observed as one goes from sample (PANI/cit-MAG)₂₅ to sample (PANI/cit-MAG)₅₀, indicating that above $\ell = 25$ the film reached a thickness higher than the correlation length of about 30 nm. These findings represent a strong support to the usefulness of the simulation approach presented here.

V. CONCLUSION

In this study nanofilms of citrate-coated maghemite nanoparticles embedded in polyaniline, (PANI/cit-MAG) _{ℓ} , were produced by the layer-by-layer technique, experimentally investigated via high resolution microscopy (HRM) and magnetization measurements (ZFC/FC and $M \times H$ curves) and employed as a model system to evaluate the effectiveness of the simulation approach herein proposed. We found the HRM data (samples morphology) in very good agreement with the results provided by the Cell Dynamic System (CDS) simulation. For a typical sample the simulated distribution function, $g(r)$, provided the first peak position at 10 nm for nanosized particles with 7.5 nm in diameter, thus leaving about 2.5 nm for the surface-to-surface distance. This simulated value is in very good agreement with the surface-to-surface distance of 3 nm obtained from the HRM micrograph.

The samples morphology provided by the CDS simulation was then used as input to Monte Carlo (MC) simulations of ZFC/FC curves and $M \times H$ loops, including energy terms corresponding to shape and crystalline magnetic anisotropy and dipolar interactions. The simulated curves presented good correspondence in several important features regarding real samples, providing good estimation and understanding for the ZFC curve maximum (T_{MAX}), remanence (M_R/M_s), and coercivity (H_C). For a typical sample we found the simulated T_{MAX} (53 K) in excellent agreement with the experimental data (54 K). Nevertheless, for a typical sample we found experimental values of remanence and coercivity systematically lower ($M_R/M_s = 0.32$ and $H_C = 210$ Oe) than the values we found in the MC simulation ($M_R/M_s = 0.53$ and $H_C = 274$ Oe). We understood that this difference is due to the particle clustering in the real samples, which is expected to lower both M_R/M_s and H_C with respect to the values for a system consisting of isolated nanoparticles.

In summary we conclude that the combination of CDS and MC simulations provided a realistic description for the as-produced nanofilms. The method developed herein can be employed to design optimized magnetic nanocomposites and to predict their respective properties with great accuracy. This novel approach would also find application in fields beyond that investigated here, spanning from biology and medicine to engineering and nanoelectronics, where phase segregated systems play a major role.

VI. ACKNOWLEDGMENTS

The financial support from the Brazilian agencies MCT-CNPq, FINEP, CAPES, is gratefully acknowledged. M. A. G. Soler thanks Professor Steve Granick (Department of Materials Science and Engineering, University of Illinois at Urbana-Champaign) for the hospitality in the period from April to June, 2009, and CAPES-Brazil (4410-08-4). The authors acknowledge the support of Dr. Michael Marshall and Dr. Vania Petrova (Frederick Seitz Materials Research Laboratory, University of Illinois at Urbana-Champaign) in the TEM and SEM measurements, Dr. Emilia C.D. Lima (Universidade Federal de Goiás, Brazil) for the preparation of nanoparticle samples and Prof. Miguel A. Novak (Universidade Federal do Rio de Janeiro, Brazil) for magnetic characterization facilities.

* Electronic address: neumann@ifufrj.br

- ¹ Jonathan A. Fan, Chihhui Wu, Kui Bao, Jiming Bao, Rizia Bardhan, Naomi J. Halas, Vinothan N. Manoharan, Peter Nordlander, Gennady Shvets, and Federico Capasso. Self-Assembled Plasmonic Nanoparticle Clusters. *SCIENCE*, 328(5982):1135–1138, MAY 28 2010.
- ² Marek Grzelczak, Jan Vermant, Eric M. Furst, and Luis M. Liz-Marzan. Directed Self-Assembly of Nanoparticles. *ACS NANO*, 4(7):3591–3605, JUL 2010.
- ³ Anna C. Balazs, Todd Emrick, and Thomas P. Russell. Nanoparticle polymer composites: Where two small worlds meet. *SCIENCE*, 314(5802):1107–1110, NOV 17 2006.
- ⁴ HS Kim, BH Sohn, W Lee, JK Lee, SJ Choi, and SJ Kwon. Multifunctional layer-by-layer self-assembly of conducting polymers and magnetic nanoparticles. *THIN SOLID FILMS*, 419(1-2):173–177, NOV 1 2002.
- ⁵ Janine Nunes, Kevin P. Herlihy, Lamar Mair, Richard Superfine, and Joseph M. DeSimone. Multifunctional Shape and Size Specific Magneto-Polymer Composite Particles. *NANO LETTERS*, 10(4):1113–1119, APR 2010.
- ⁶ Subhankar Bedanta and Wolfgang Kleemann. Supermagnetism. *JOURNAL OF PHYSICS D-APPLIED PHYSICS*, 42(1), JAN 7 2009.
- ⁷ Georgia C. Papaefthymiou. Nanoparticle magnetism. *NANO TODAY*, 4(5):438–447, OCT 2009. 1st Nano Today Conference, Singapore, SINGAPORE, AUG 02-05, 2009.
- ⁸ Aldo F. Rebolledo, Antonio B. Fuertes, Teresita Gonzalez-Carreno, Marta Sevilla, Teresa Valdes-Solis, and Pedro Tartaj. Signatures of clustering in superparamagnetic colloidal nanocomposites of an inorganic and hybrid nature. *SMALL*, 4(2):254–261, FEB 2008.
- ⁹ PJ Jensen and GM Pastor. Low-energy properties of two-dimensional magnetic nanostructures: interparticle interactions and disorder effects. *NEW JOURNAL OF PHYSICS*, 5, JUN 12 2003.
- ¹⁰ R. Skomski. *Simple Models of Magnetism*. Oxford University Press, New York, 2008.
- ¹¹ RW Chantrell, GN Coverdale, M ElHilo, and K OGrady. Modelling of interaction effects in fine particle systems. *JOURNAL OF MAGNETISM AND MAGNETIC MATERIALS*, 157:250–255, MAY 1996. 6th European Magnetic Materials and Applications Conference (EMMA 95), TU VIENNA, VIENNA, AUSTRIA, SEP 04-08, 1995.
- ¹² M Bahiana, JPP Nunes, D Altbir, P Vargas, and M Knobel. Ordering effects of the dipolar interaction in lattices of small magnetic particles. *JOURNAL OF MAGNETISM AND MAGNETIC MATERIALS*, 281(2-3):372–377, OCT 2004.
- ¹³ CSM Bastos, M Bahiana, WC Nunes, MA Novak, D Altbir, P Vargas, and M Knobel. Role of the alloy structure in the magnetic behavior of granular systems. *PHYSICAL REVIEW B*, 66(21), DEC 1 2002.
- ¹⁴ DA Dimitrov and GM Wysin. Magnetic properties of superparamagnetic particles by a Monte Carlo method. *PHYSICAL REVIEW B*, 54(13):9237–9241, OCT 1 1996.
- ¹⁵ JL Dormann, L Spinu, E Tronc, JP Jolivet, F Lucari, and F D’Orazio. Effect of interparticle interactions on the dynamical properties of gamma-Fe₂O₃ nanoparticles. *JOURNAL OF MAGNETISM AND MAGNETIC MATERIALS*, 183(3):L255–L260, MAR 1998.
- ¹⁶ J Garcia-Otero, M Porto, J Rivas, and A Bunde. Influence of dipolar interaction on magnetic properties of ultrafine ferromagnetic particles. *PHYSICAL REVIEW LETTERS*, 84(1):167–170, JAN 3 2000.
- ¹⁷ O Iglesias and A Labarta. Magnetic relaxation in terms of microscopic energy barriers in a model of dipolar interacting nanoparticles. *PHYSICAL REVIEW B*, 70(14), OCT 2004.
- ¹⁸ D Kechrakos and KN Trohidou. Monte Carlo study of the magnetic behavior of self-assembled nanoparticles. *JOURNAL OF MAGNETISM AND MAGNETIC MATERIALS*, 295(2):177–179, AUG 2005. International Conference on Magnetism (ICM 2003), Rome, ITALY, JUL 27-AUG 01, 2003.

- ¹⁹ JJ Weis. Simulation of quasi-two-dimensional dipolar systems. *JOURNAL OF PHYSICS-CONDENSED MATTER*, 15(15):S1471–S1495, APR 23 2003.
- ²⁰ M. C. Bujan-Nunez, N. Fontaina-Troertino, C. Vazquez-Vazquez, M. A. Lopez-Quintela, Y. Pineiro, D. Serantes, D. Baldomir, and J. Rivas. Influence of the nanoparticle size on the blocking temperature of interacting systems: Monte Carlo simulations. *JOURNAL OF NON-CRYSTALLINE SOLIDS*, 354(47-51):5222–5223, DEC 1 2008. 9th International Workshop on Non Crystalline Solids, Univ Porto, Dept Phys, Porto, PORTUGAL, APR 27-30, 2008.
- ²¹ Cristina E. Hoppe, Francisco Rivadulla, M. Arturo Lopez-Quintela, M. Carmen Bujan, Jose Rivas, David Serantes, and Daniel Baldomir. Effect of submicrometer clustering on the magnetic properties of free-standing superparamagnetic nanocomposites. *JOURNAL OF PHYSICAL CHEMISTRY C*, 112(34):13099–13104, AUG 28 2008.
- ²² S Lamba and S Annapoorni. Single domain magnetic arrays: role of disorder and interactions. *EUROPEAN PHYSICAL JOURNAL B*, 39(1):19–25, MAY 2004.
- ²³ Y. Oono and S. Puri. Study of phase-separation dynamics by use of Cell Dynamical Systems. I. Modeling. *Phys. Rev. A*, 38:434–453, Jul 1988.
- ²⁴ S. Puri and Y. Oono. Study of phase-separation dynamics by use of Cell Dynamical Systems. II. Two-dimensional demonstrations. *Phys. Rev. A*, 38:1542–1565, Aug 1988.
- ²⁵ Leonardo G. Paterno, Maria A. G. Soler, Fernando J. Fonseca, Joao P. Sinnecker, Elis H. C. P. Sinnecker, Emilia C. D. Lima, Sonia N. Bao, Miguel A. Novak, and Paulo C. Morais. Magnetic Nanocomposites Fabricated via the Layer-by-Layer Approach. *JOURNAL OF NANOSCIENCE AND NANOTECHNOLOGY*, 10(4):2679–2685, APR 2010. 2nd International Conference on Advanced Nano Materials, Univ Aveiro, Aveiro, PORTUGAL, 2008.
- ²⁶ Leonardo G. Paterno, Maria A. G. Soler, Fernando J. Fonseca, Joao P. Sinnecker, Elis H. C. P. Sinnecker, Emilia C. D. Lima, Miguel A. Novak, and Paulo C. Morais. Layer-by-Layer Assembly of Bifunctional Nanofilms: Surface-Functionalized Maghemite Hosted in Polyaniline. *JOURNAL OF PHYSICAL CHEMISTRY C*, 113(13):5087–5095, APR 2 2009.
- ²⁷ P. C. Morais, R. L. Santos, A. C. M. Pimenta, R. B. Azevedo, and E. C. D. Lima. Preparation and characterization of ultra-stable biocompatible magnetic fluids using citrate-coated cobalt ferrite nanoparticles. *THIN SOLID FILMS*, 515(1):266–270, SEP 25 2006. International Conference on Surfaces, Coatings and Nanostructured Materials (nanoSMat), Univ Aveiro, Aveiro, PORTUGAL, SEP 07-09, 2005.
- ²⁸ J POPPLEWELL and L SAKHNINI. THE DEPENDENCE OF THE PHYSICAL AND MAGNETIC-PROPERTIES OF MAGNETIC FLUIDS ON PARTICLE-SIZE. *JOURNAL OF MAGNETISM AND MAGNETIC MATERIALS*, 149(1-2):72–78, AUG 1995. 7th International Conference on Magnetic Fluids (ICMF-VII), BHAVNAGAR, INDIA, JAN 07-14, 1995.
- ²⁹ DM SHERMAN and TD WAITE. ELECTRONIC-SPECTRA OF FE-3+ OXIDES AND OXIDE HYDROXIDES IN THE NEAR IR TO NEAR UV. *AMERICAN MINERALOGIST*, 70(11-12):1262–1269, NOV-DEC 1985.
- ³⁰ M BAHIANA and Y OONO. CELL DYNAMIC SYSTEM APPROACH TO BLOCK COPOLYMERS. *PHYSICAL REVIEW A*, 41(12):6763–6771, JUN 15 1990.
- ³¹ A SHINOZAKI and Y OONO. SPINODAL DECOMPOSITION IN 3-SPACE. *PHYSICAL REVIEW E*, 48(4):2622–2654, OCT 1993.
- ³² J HOSHEN and R KOPELMAN. PERCOLATION AND CLUSTER DISTRIBUTION .1. CLUSTER MULTIPLE LABELING TECHNIQUE AND CRITICAL CONCENTRATION ALGORITHM. *PHYSICAL REVIEW B*, 14(8):3438–3445, 1976.
- ³³ BD Cullity and CD Graham. *Introduction to Magnetic Materials*. Wiley-IEEE Press; 2 edition, 2008.
- ³⁴ P Dutta, A Manivannan, MS Seehra, N Shah, and GP Huffman. Magnetic properties of nearly defect-free maghemite nanocrystals. *PHYSICAL REVIEW B*, 70(17), NOV 2004.
- ³⁵ PV HENDRIKSEN, F BODKER, S LINDEROTH, S WELLS, and S MORUP. ULTRAFINE MAGHEMITE PARTICLES .1. STUDIES OF INDUCED MAGNETIC TEXTURE. *JOURNAL OF PHYSICS-CONDENSED MATTER*, 6(16):3081–3090, APR 18 1994.
- ³⁶ R Hergt, R Hiergeist, I Hilger, WA Kaiser, Y Lapatinikov, S Margel, and U Richter. Maghemite nanoparticles with very high AC-losses for application in RF-magnetic hyperthermia. *JOURNAL OF MAGNETISM AND MAGNETIC MATERIALS*, 270(3):345–357, APR 2004.
- ³⁷ T JONSSON, J MATTSSON, C DJURBERG, FA KHAN, P NORDBLAD, and P SVEDLINDH. AGING IN A MAGNETIC PARTICLE SYSTEM. *PHYSICAL REVIEW LETTERS*, 75(22):4138–4141, NOV 27 1995.
- ³⁸ B Martinez, X Obradors, L Balcells, A Rouanet, and C Monty. Low temperature surface spin-glass transition in gamma-Fe₂O₃ nanoparticles. *PHYSICAL REVIEW LETTERS*, 80(1):181–184, JAN 5 1998.
- ³⁹ B Martinez, A Roig, X Obradors, E Molins, A Rouanet, and C Monty. Magnetic properties of gamma-Fe₂O₃ nanoparticles obtained by vaporization condensation in a solar furnace. *JOURNAL OF APPLIED PHYSICS*, 79(5):2580–2586, MAR 1 1996.
- ⁴⁰ T. N. Shendruk, R. D. Desautels, B. W. Southern, and J. van Lierop. The effect of surface spin disorder on the magnetism of gamma-Fe₂O₃ nanoparticle dispersions. *NANOTECHNOLOGY*, 18(45), NOV 14 2007.
- ⁴¹ JK VASSILIOU, V MEHROTRA, MW RUSSELL, EP GIANNELIS, RD MCMICHAEL, RD SHULL, and RF ZIOLO. MAGNETIC AND OPTICAL-PROPERTIES OF GAMMA-FE₂O₃ NANOCRYSTALS. *JOURNAL OF APPLIED PHYSICS*, 73(10, Part 1):5109–5116, MAY 15 1993.
- ⁴² U Nowak, RW Chantrell, and EC Kennedy. Monte Carlo simulation with time step quantification in terms of Langevin dynamics. *PHYSICAL REVIEW LETTERS*, 84(1):163–166, JAN 3 2000.
- ⁴³ C Papusoi. The particle interaction effects in the field-cooled and zero-field-cooled magnetization processes. *JOURNAL OF MAGNETISM AND MAGNETIC MATERIALS*, 195(3):708–732, JUN 1999.
- ⁴⁴ EC STONER and EP WOHLFARTH. A MECHANISM OF MAGNETIC HYSTERESIS IN HETEROGENEOUS ALLOYS.

PHILOSOPHICAL TRANSACTIONS OF THE ROYAL SOCIETY OF LONDON SERIES A-MATHEMATICAL AND PHYSICAL SCIENCES, 240(826):599–642, 1948.

- ⁴⁵ M El-Hilo, RW Chantrell, and K O’Grady. A model of interaction effects in granular magnetic solids. *JOURNAL OF APPLIED PHYSICS*, 84(9):5114–5122, NOV 1 1998.

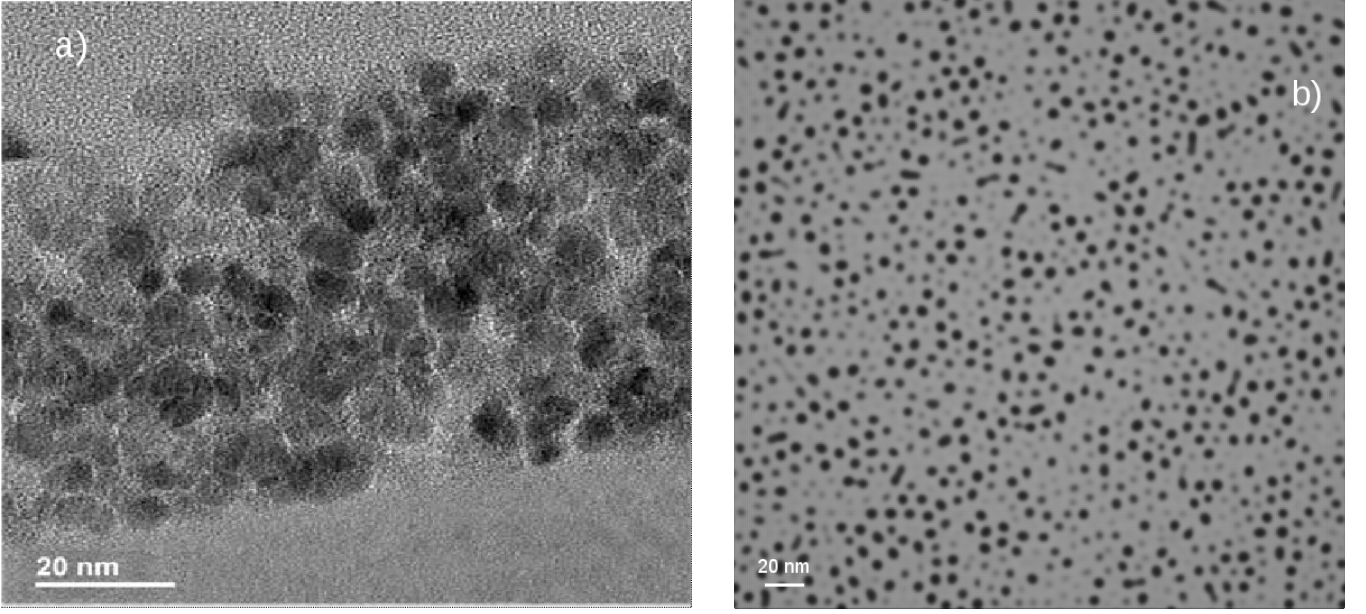


FIG. 1: Typical surface morphology of a (PANI/cit-MAG)₁₀ film (a) and simulated (b) cross-section structure after CDS modeling.

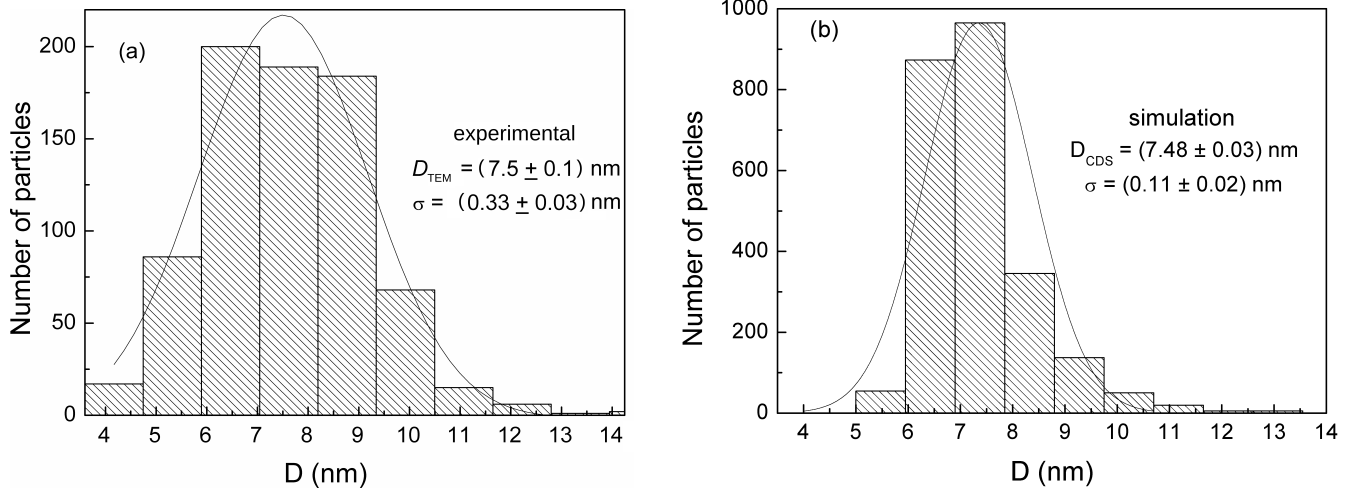


FIG. 2: (a) Particle size histogram of the cit-MAG colloidal sample, obtained from the TEM images. The solid line results from the curve-fitting of the data using the log-normal distribution function. (b) Particle size histogram of the average particle diameter after CDS simulation.

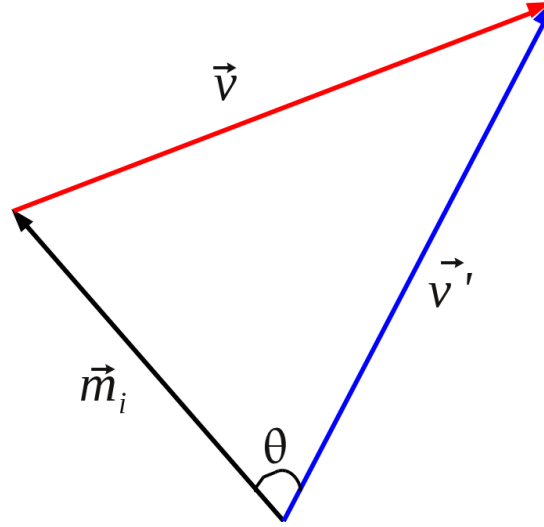


FIG. 3: At each trial step a magnetic moment \vec{m}_i (black) is selected. A random vector \vec{v} with modulus $G|\vec{m}_i|$ (red) is added to the latter. The resulting vector \vec{v}' (blue) gives the direction of the new magnetic moment. After rescaling it in order to keep the same modulus as \vec{m}_i , it will be the new magnetic moment \vec{m}'_i . We can control the angle θ between \vec{m}_i and \vec{m}'_i by choosing the appropriate G .

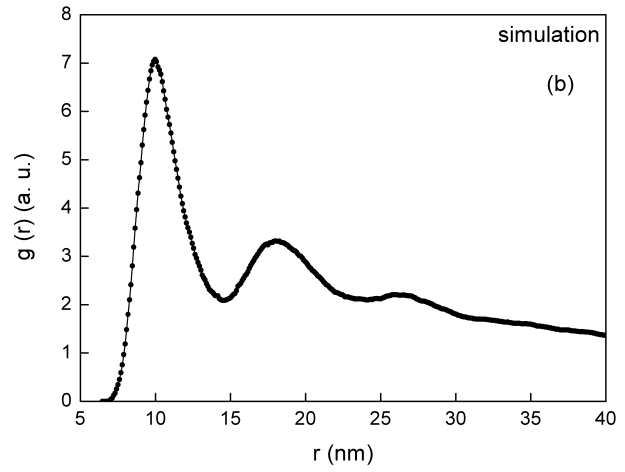
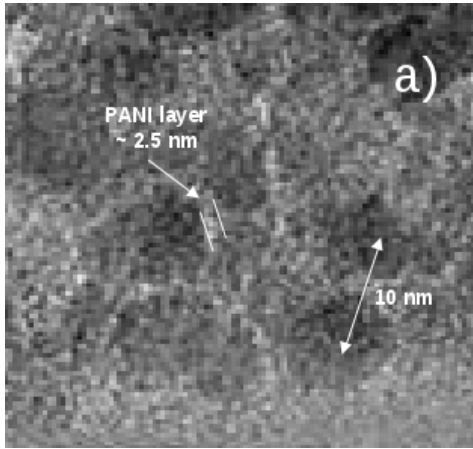


FIG. 4: Typical cross-section TEM micrograph of a (PANI/cit-MAG)₁₀ film (a); and simulated pair distribution function, $g(r)$, for the $300 \times 300 \times 30$ grid (b).

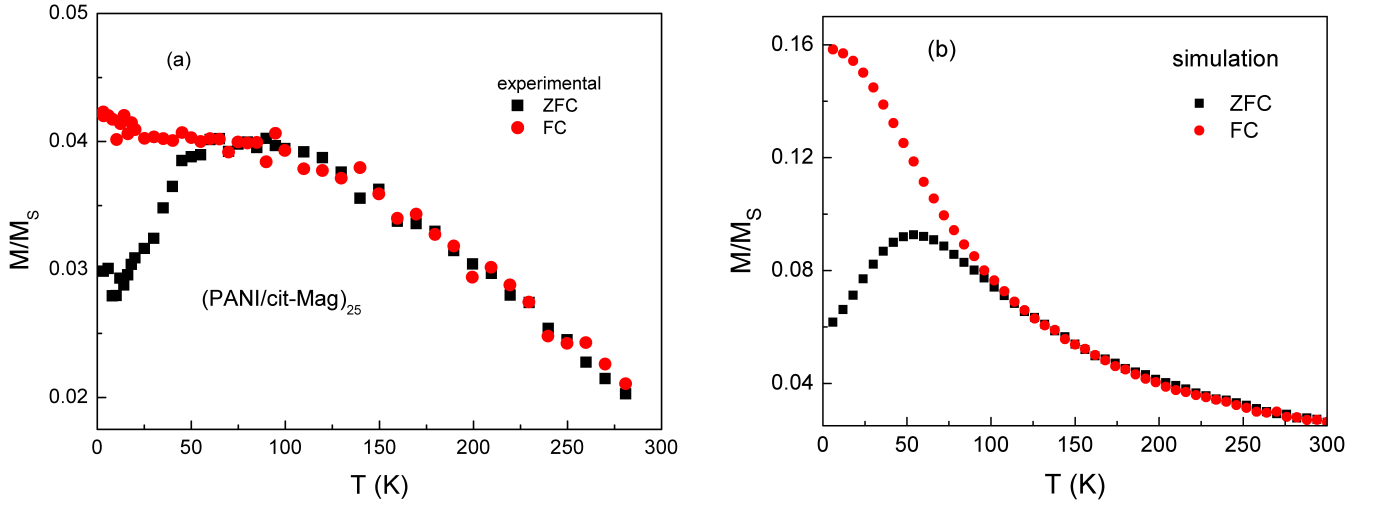


FIG. 5: Experimental (PANI/cit-MAG)₂₅ nanofilm (a) and simulated (b) ZFC/FC curves obtained at a steady field of 36 Oe. Solid lines on (b) are guide to the eyes only.

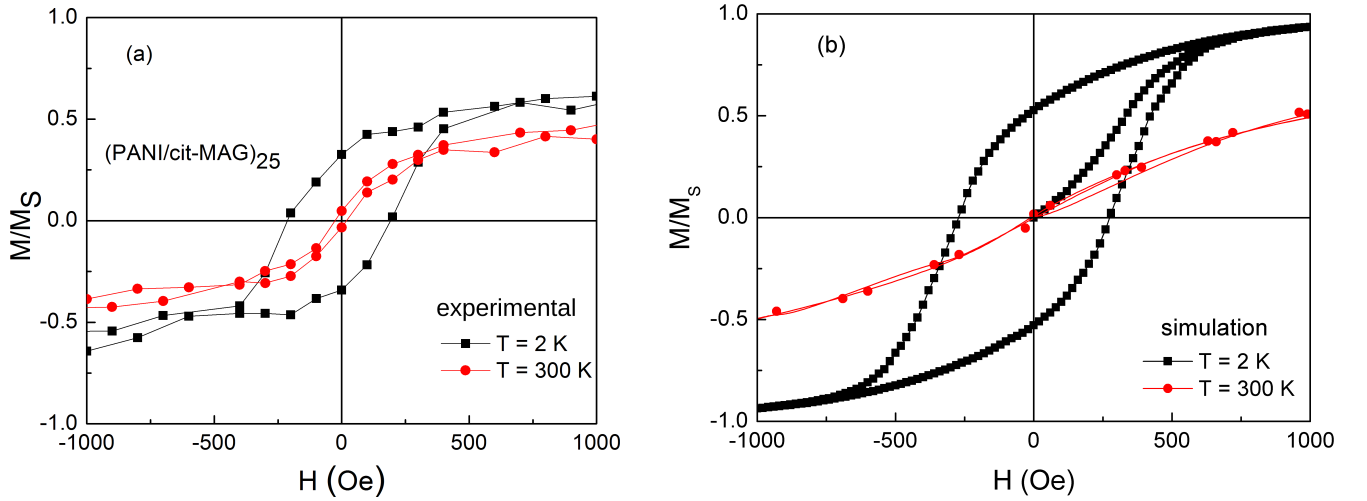


FIG. 6: Experimental (PANI/cit-MAG)₂₅ nanofilm (a) and simulated (b) hysteresis curves at different temperatures. Solid lines on (b) are guide to the eyes only.